# The C-Terminal Segment of Yeast BMH Proteins Exhibits Different Structure Compared to Other 14-3-3 Protein Isoforms

**ARTICLE** *in* BIOCHEMISTRY · APRIL 2010

Impact Factor: 3.02 · DOI: 10.1021/bi100273k · Source: PubMed



**8 AUTHORS**, INCLUDING:

Dana Veisova
Academy of Sciences of the Czech Republic
**4** PUBLICATIONS **43** CITATIONS
SEE PROFILE

Miroslav Stepánek
Charles University in Prague
**56** PUBLICATIONS **712** CITATIONS
SEE PROFILE

Tomas Obsil
Charles University in Prague
**66** PUBLICATIONS **1,908** CITATIONS
SEE PROFILE

Veronika Obsilova
Academy of Sciences of the Czech Republic
**35** PUBLICATIONS **766** CITATIONS
SEE PROFILE

BIOCHEMISTRY
including biophysical chemistry & molecular biology
Article

*Biochemistry* **2010,** *49,* 3853–3861 3853
DOI: 10.1021/bi100273k

# The C-Terminal Segment of Yeast BMH Proteins Exhibits Different Structure Compared to Other 14-3-3 Protein Isoforms†

Dana Veisova,[‡] Lenka Rezabkova,[‡,§] Miroslav Stepanek,[§] Pavlina Novotna,[⊥] Petr Herman,[∥] Jaroslav Vecer,[∥] Tomas Obsil,[‡,§] and Veronika Obsilova*[,‡]

[‡]*Institute of Physiology, Academy of Sciences of the Czech Republic, 14220 Prague, Czech Republic,* [§]*Department of Physical and Macromolecular Chemistry, Faculty of Science, Charles University, 12843 Prague, Czech Republic,* [∥]*Faculty of Mathematics and Physics, Institute of Physics, Charles University, 12116 Prague, Czech Republic, and* [⊥]*Department of Analytical Chemistry, Institute of Chemical Technology, 16628 Prague, Czech Republic*

*Received February 23, 2010; Revised Manuscript Received April 9, 2010*

ABSTRACT: Yeast 14-3-3 protein isoforms BMH1 and BMH2 possess a distinctly variant C-terminal tail which differentiates them from the isoforms of higher eukaryotes. Their C-termini are longer and contain a polyglutamine stretch of unknown function. It is now well established that the C-terminal segment of 14-3-3 proteins plays an important regulatory role by functioning as an autoinhibitor which occupies the ligand binding groove and blocks the binding of inappropriate ligands. Whether the same holds true or not for the yeast isoforms is unclear. Therefore, we investigated the conformational behavior of the C-terminal segment of BMH proteins using various biophysical techniques. Dynamic light scattering, sedimentation velocity, time-resolved fluorescence anisotropy decay, and size exclusion chromatography measurements showed that the molecules of BMH proteins are significantly larger compared to the human 14-3-3ζ isoform. On the other hand, the sedimentation analysis confirmed that BMH proteins form dimers. Time-resolved tryptophan fluorescence experiments revealed no dramatic structural changes of the C-terminal segment upon the ligand binding. Taken together, the C-terminal segment of BMH proteins adopts a widely opened and extended conformation that makes difficult its folding into the ligand binding groove, thus increasing the apparent molecular size. It seems, therefore, that the C-terminal segment of BMH proteins does not function as an autoinhibitor.

The 14-3-3 proteins have attracted quite an attention over the past decade mainly due to the variety of biological processes they participate in, including cell cycle regulation, metabolism control, apoptosis, and control of gene transcription (*1*−*3*). More than 300 different cellular proteins from diverse eukaryotic organisms have been described as binding partners for the 14-3-3 proteins by now. 14-3-3 proteins are highly conserved dimeric proteins with a molecular mass about 30 kDa (for a monomer) found in all eukaryotes. They function as scaffold molecules modulating the activity of their binding partners. The 14-3-3 proteins form cup-shaped mono- or heterodimers in the center of which is located a large 40 Å wide deep channel containing two amphipatic grooves through which 14-3-3 proteins bind their substrates mostly in a phosphorylation-dependent manner (*4*, *5*).

Many organisms express multiple isoforms: in mammals seven isoforms have been identified, plants contain up to 13 isoforms, and in yeasts just two isoforms have been recognized (*3*, *6*). The presence of multiple 14-3-3 isoforms over the wide range of species suggests that individual isoforms can interact with different targets. The whole molecule of the 14-3-3 dimer is very rigid; the most flexible region is its C-terminal segment where the individual 14-3-3 isoforms show the highest sequence variability. It is now well established that this C-terminal segment plays an important regulatory role by functioning as an autoinhibitor which can occupy the ligand binding groove and blocks the binding of inappropriate ligands (Figure 1A) (*7*−*10*). Differences in the sequence of the C-terminal segment of individual 14-3-3 isoforms and also their different interaction with the ligand binding groove might significantly contribute to the uniqueness of the individual isoform binding properties and functional diversity.

Two 14-3-3 protein homologues from *Saccharomyces cerevisiae* BMH1 and BMH2 possess a distinctly variant C-terminal segment which differentiates them from the seven mammalian isoforms (*6*, *11*). Their C-terminus is longer and contains a polyglutamine stretch of unknown function (Figure 1B). The polyglutamine (polyQ) sequences of certain proteins are known to induce protein aggregation that underlies the cytotoxicity of these molecules. It has been shown that peptides containing polyQ stretches adopt β-structure and can form β-sheets (both antiparallel and parallel), β-hairpins, and also highly compact random coil (*12*).

The autoinhibitory function of the C-terminal segment of 14-3-3 isoforms from higher eukaryotes is now well established. Whether the same holds true or not for the yeast isoforms is unclear. Therefore, we investigated the conformational behavior of the C-terminal segment of BMH proteins using various biophysical techniques. Dynamic light scattering, sedimentation velocity, time-resolved fluorescence anisotropy decay, and size

†This work was supported by Grant IAA501110801 of the Grant Agency of the Academy of Sciences of the Czech Republic, by Research Projects MSM0021620857 and MSM0021620835 and Centre of Neurosciences LC554 of the Ministry of Education, Youth, and Sports of the Czech Republic, and by Research Project AV0Z50110509 of the Academy of Sciences of the Czech Republic.

*To whom the correspondence should be addressed. Tel: 420-241062191. Fax: 420-244472269. E-mail: obsilova@biomed.cas.cz.


Published on Web 04/12/2010

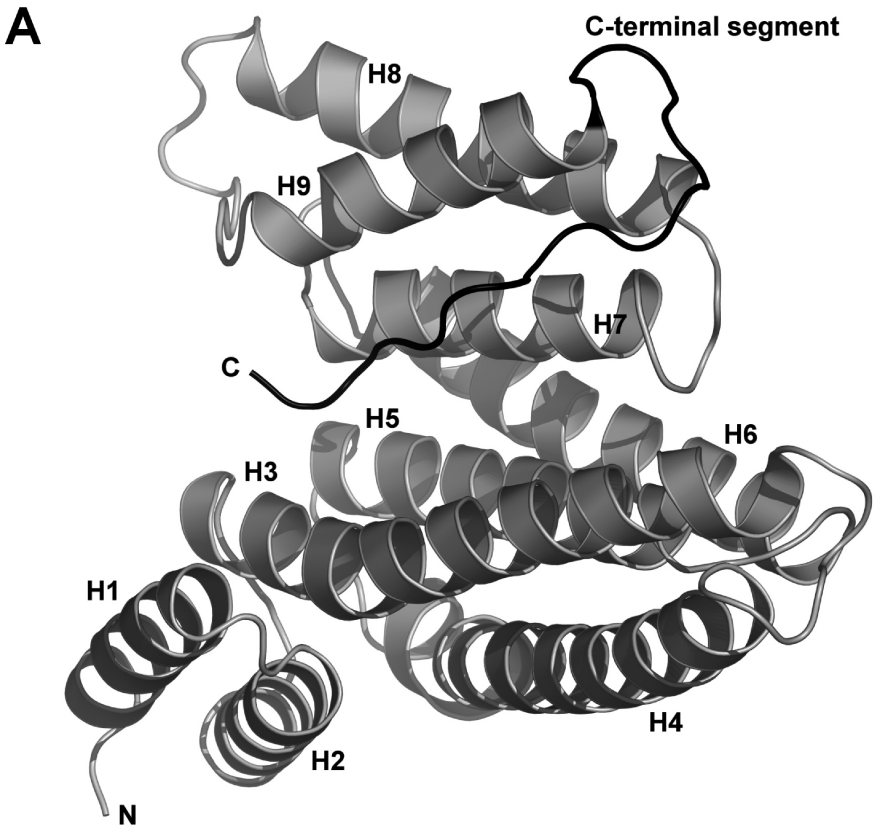


**B**

```
BMH1      MSTSREDSVYLAKLAEQAERYEEMVENMKTVASSGQELSVEERNLLSVAY
BMH2      MSQTREDSVYLAKLAEQAERYEEMVENMKAVASSGQELSVEERNLLSVAY
14-3-3ζ   --MDKNELVQKAKLAEQAERYDDMAACMKSVTEQGAELSNEERNLLSVAY

BMH1      KNVIGARRASWRIVSSIEQKEESKEKSEHQVELICSYRSKIETELTKISD
BMH2      KNVIGARRASWRIVSSIEQKEESKEKSEHQVELIRSYRSKIETELTKISD
14-3-3ζ   KNVVGARRSSWRVVSSIEQKTEGAEK---KQQMAREYREKIETELRDICN

BMH1      DILSVLDSHLIPSATTGESKVFYYKMKGDYHRYLAEFSSGDAREKATNAS
BMH2      DILSVLDSHLIPSATTGESKVFYYKMKGDYHRYLAEFSSGDAREKATNSS
14-3-3ζ   DVLSLLEKFLIPNASQAESKVFYLKMKGDYYRYLAEVAAGDDKKGIVDQS

BMH1      LEAYKTASEIATTELPPTHPIRLGLALNFSVFYYEIQNSPDKACHLAKQA
BMH2      LEAYKTASEIATTELPPTHPIRLGLALNFSVFYYEIQNSPDKACHLAKQA
14-3-3ζ   QQAYQEAFEISKKEMQPTHPIRLGLALNFSVFYYEILNSPEKACSLAKTA

BMH1      FDDAIAELDTLSEESYKDSTLIMQLLRDNLTLWTSDMSESGQAEDQQQQQ
BMH2      FDDAIAELDTLSEESYKDSTLIMQLLRDNLTLWTSDISESGQEDQQQQQQ
14-3-3ζ   FDEAIAELDTLSEESYKDSTLIMQLLRDNLTLWTSDTQGDEAEAGEGGEN

BMH1      QHQQQQ------PPAAAEGEAPK
BMH2      QQQQQQQQQQQQAPAEQTQGEPTK
14-3-3ζ   -----------------------
```

FIGURE 1: C-Terminal segment of the 14-3-3 protein. (A) Structure of the human 14-3-3 protein isoform ζ (*24*) (shown in gray) with the modeled C-terminal segment located within the ligand binding groove (shown in black) (*9*). (B) Sequence alignment of yeast BMH proteins and human 14-3-3ζ. The following sequences were used: the *S. cerevisiae* BMH1 protein (accession number P29311), the *S. cerevisiae* BMH2 protein (accession number P34730), and the human isoform ζ (accession number P63104). Sequence alignments were performed using the ClustalW program (*25*). Conserved regions are shaded in gray. The positions where the stop codons were inserted are underlined and in boldface. The boldfaced residues in squares were mutated to tryptophans.

exclusion chromatography measurements showed that an apparent size of the molecules of BMH proteins is significantly bigger compared to the human 14-3-3ζ isoform. On the other hand, the sedimentation equilibrium analysis proved that BMH proteins form dimers as other 14-3-3 protein isoforms. Time-resolved tryptophan fluorescence experiments revealed no dramatic structural changes of the C-terminal segment upon the ligand binding. Our results indicate that the C-terminal segment of BMH proteins adopts very open and extended conformation that makes difficult its folding into the ligand binding groove, thus

increasing the apparent molecular size. It seems, therefore, that the C-terminal segment of BMH proteins does not function as an autoinhibitor.

## MATERIALS AND METHODS

*Expression and Purification of BMH Proteins*. DNA encoding *S. cerevisiae* BMH1 and BMH2 proteins were ligated into pET-15b (Novagen) using the *Nde*I and *Bam*HI sites. The entire coding region was checked by sequencing. All mutants were generated using the QuickChange Kit (Stratagene). To generate C-terminally truncated (ΔC) mutants of BMH1 and BMH2, a stop codon was introduced instead of $Met^{237}$ and $Ile^{237}$, respectively. The BMH proteins and human 14-3-3ζ protein were expressed and purified as described previously (*13*).

*Labeling of BMH Proteins by 1,5-IAEDANS*. Covalent modification of BMH proteins with the thiol-reactive probe 1,5-IAEDANS[1] was carried out as described previously (*14*). Briefly, the protein (50−70 μM) in 20 mM Tris-HCl (pH 7.5), 150 mM NaCl, and label was mixed at a molar ratio of 1:40 and incubated at 30 °C for 2 h and then at 4 °C overnight in the dark. The incorporation stoichiometry was determined by comparing the peak protein absorbance at 280 nm with the absorbance of bound 1,5-IAEDANS measured at 336 nm using an extinction coefficient of 5700 $M^{-1}$ $cm^{-1}$ (Molecular Probes, Eugene, OR).

*Size Exclusion Chromatography* (*SEC*). Size exclusion chromatography on a Superdex 200 HR 10/30 column (Amersham Biosciences) was performed in buffer containing 20 mM Tris-HCl (pH 7.5), 200 mM NaCl, 1 mM EDTA, and 5 mM DTT. All experiments were carried out at 4 °C with a flow rate of 0.5 mL/min.

*Analytical Ultracentrifugation* (*AUC*). Sedimentation equilibrium (SE) and sedimentation velocity (SV) experiments were performed using a ProteomLab XL-I, Beckman Coulter analytical ultracentrifuge. Sedimentation equilibrium experiments of the BMH1, BMH2, and 14-3-3ζ (WT and ΔC mutants) were conducted at loading concentrations of 10 μM, 4 °C, and rotor speeds ranging from 10500 to 16500 rpm. Sedimentation velocity experiments were conducted at loading concentrations of 17 μM, 4 °C, and rotor speed 40000 rpm. All data were collected at 280 nm. Samples were dialyzed against the buffer containing 20 mM Tris-HCl (pH 7.5), 150 mM NaCl, and 2 mM 2-mercaptoethanol prior to analysis. Data were analyzed using the SEDFIT and SEDPHAT packages (*15*, *16*).

*Dynamic Light Scattering* (*DLS*). The light scattering setup (ALV, Langen, Germany) consisted of a 22 mW He−Ne laser operating at the wavelength $\lambda = 632.8$ nm, an ALV CGS/8F goniometer, an ALV High QE APD detector, and an ALV 5000/EPP multibit, multitau autocorrelator. Measurements were performed at the temperature of 25 °C, and the scattering angle $\theta = 90°$. All samples were measured at four different concentrations (4, 2, 1, and 0.5 mg/mL) to get a gradient in a buffer containing 20 mM Tris-HCl (pH 7.5), 150 mM NaCl, and 2 mM 2-mercaptoethanol. The DLS data, i.e., the scattered light intensities, $I(t)$, at time $t$, were evaluated by means of fitting the normalized intensity autocorrelation functions:

$$g^{(2)}(\tau) = \frac{\langle I(t)I(t+\tau)\rangle}{\langle I(t)\rangle^2} \quad (1)$$

where $\tau$ is the lag time to the equation:

$$g^{(2)}(\tau) = 1+\beta\left[\int_0^\infty A(\tau_r)\exp\left(-\frac{\tau}{\tau_r}\right)\mathrm{d}\tau_r\right]^2 \quad (2)$$

where $\beta$ is the coherence factor and $A(\tau_r)$ is the distribution function of relaxation times, $\tau_r$. The fitting was performed using the inverse Laplace transform (ILT) by means of a constrained regularization algorithm (CONTIN). The hydrodynamic radii of the protein molecules were calculated from the mean relaxation times of the corresponding diffusive modes in the CONTIN distributions, $\langle\tau_r\rangle$, according to the formula:

$$R_H = \frac{8\pi n_0^2 k_B T}{3\eta_0\lambda^2}\sin^2\left(\frac{\theta}{2}\right)\langle\tau_r\rangle \quad (3)$$

where $n_0$ and $\eta_0$, respectively, are the refractive index and viscosity of the solvent, $k_B$ is the Boltzmann constant, and $T$ is the temperature.

*Fluorescence Anisotropy-Based Binding Assay*. Steady-state fluorescence anisotropy measurements were performed on a PerkinElmer Life Sciences LS50B fluorescence spectrometer at 22 °C with 0.4 μM phosphopeptide Flc-pRaf-259 labeled with fluorescein at the N-terminus. Increasing amounts of protein were titrated into the cuvette. At each BMH concentration, the steady-state fluorescence anisotropy of fluorescein was recorded (excitation at 495 nm and emission at 520 nm). Anisotropy was calculated from the fluorescence intensities according to the relationship $r = (I_{II} - I_\perp)/(I_{II} + 2I_\perp)$. The fraction of peptide bound ($F_B$) was calculated from

$$F_B = (r_{obs} - r_{min})/[(r_{max} - r_{obs})Q + (r_{obs} - r_{min})] \quad (4)$$

where $Q$ represents the quantum yield ratio of the bound to the free form (*17*); it was estimated by calculating the ratio of the intensities of the bound to the free fluorophore. Parameter $r_{max}$ is the anisotropy at saturation, $r_{obs}$ is the observed anisotropy for any BMH concentration, and $r_{min}$ is the minimum observed anisotropy of the free phosphopeptide. $F_B$ was plotted against the BMH protein concentration and fitted using eq 5 to determine the $K_D$ for BMH/pRaf-259 complex formation (*18*):

$$F_B = \frac{K_D + [P1] + [P2] - \sqrt{(K_D + [P1] + [P2])^2 - 4[P1][P2]}}{2[P1]} \quad (5)$$

where $K_D$ is the equilibrium dissociation constant, [P1] is the Flc-pRaf-259 concentration, and [P2] is the BMH concentration. Nonlinear data fitting was performed using the Origin 6.0 package (MicroCal Software Inc.).

*Time-Resolved Fluorescence Measurements*. Fluorescence intensity and anisotropy decays were measured on a time-correlated single photon counting apparatus as described previously (*8*). The fluorescence decays have been acquired under the "magic angle" conditions when the measured intensity decay, $I(t)$, is independent of the rotational diffusion of the chromophore and provides unbiased information about lifetimes. The apparatus response function was measured with a diluted Ludox

[1]Abbreviations: 1,5-IAEDANS, 5-((((2-iodoacetyl)amino)ethyl)amino)-naphthalene-1-sulfonic acid; AEDANS, 5-(((acetylamino)ethyl)amino)-naphthalene-1-sulfonic acid; AUC, analytical ultracentrifugation; CD, circular dichroism; DLS, dynamic light scattering; DTT, dithiothreitol; FLC, fluorescein; SE, sedimentation equilibrium; SEC, size exclusion chromatography; SV, sedimentation velocity; SVD-MEM, singular value decomposition maximum entropy method; WT, wild type.

(colloidal silica) solution. Samples were placed in a thermostatic holder, and all experiments were performed at 22 °C in a buffer containing 20 mM Tris-HCl (pH 7.5), 150 mM NaCl, and 1 mM EDTA. The protein concentration was 15 $\mu$M. Dansyl fluorescence was excited at 315 nm by an actively mode-locked picosecond dye laser (Spectra Physics). Fluorescence was collected at 480 nm using a monochromator with a 400 nm cutoff filter placed in front of its input slit. Tryptophan emission was excited at 298 nm and collected at 355 nm through a monochromator complemented by a UG1 glass filter (Zeiss) in front of the input slit. Fluorescence was assumed to decay multiexponentially according to the formula:

$$I(t) = \sum_i \alpha_i e^{-t/\tau_i} \quad (6)$$

where $\tau_i$ and $\alpha_i$ are the fluorescence lifetimes and the corresponding amplitudes, respectively. $I(t)$ was analyzed by the singular value decomposition maximum entropy method (SVD-MEM) coded according to Bryan (*19*). Tests of the used SVD-MEM functionality were published recently (*20*). The program yields a set of amplitudes $\alpha_i$ that represents the lifetime distribution in the decay. We have chosen 100 lifetimes covering the range from 20 ps to 20 ns for tryptophan and 50 ns for the AEDANS fluorescence. The lifetimes were equidistantly spaced in the logarithmic scale. Not having prior information about the number of lifetime classes (peaks) in the lifetime distribution and about the distribution shape, the data analysis started from the flat initial guess where all lifetimes have the same prior probability. The mean lifetime $\tau_{mean}$ was calculated as

$$\tau_{mean} = \sum_i f_i \tau_i \quad (7)$$

where $f_i$ is the fractional intensity of the $i$th lifetime component

$$f_i = \alpha_i \tau_i / \sum_i \alpha_i \tau_i \quad (8)$$

The measured parallel $I_{||}(t)$ and perpendicular $I_{\perp}(t)$ decays were analyzed globally using the SVD-MEM approach, similarly to decay data, to find parameters of the anisotropy decays modeled as

$$r(t) = \sum_i \beta_i e^{-t/\phi_i} \quad (9)$$

where the amplitudes $\beta_i$ represent the distribution of the correlation times $\phi_i$. $\beta_i$ are related to the initial anisotropy $r_0$ by the formula:

$$\sum \beta_i = r_0 \quad (10)$$

We used 100 correlation times $\phi_i$ equidistantly spaced in the logarithmic scale and ranging from 100 ps to 200 ns for tryptophan and 500 ns for AEDANS fluorescence.

*Circular Dichroism Measurements*. Circular dichroism measurements were carried out using a JASCO J-810 spectropolarimeter (Japan). The UV CD spectra were measured from 200 to 270 nm at a scanning speed of 100 nm/min in a quartz optical cell with a path length of 0.1 cm (Starna, USA). Other conditions of measurement were as follows: a response time of 1 s and sensitivity of 1000 mdeg. All spectra were recorded in 0.5 nm wavelength increments with a 1.0 nm bandwidth and were corrected for background by subtraction of appropriate buffer blanks. The final spectra were an average of 10 scans recorded at room temperature (23 °C). The protein concentration was 0.18−0.21 mg·mL$^{-1}$ in 20 mM Tris-HCl (pH 7.5)], 150 mM NaCl, 2 mM 2-mercaptoethanol, 10% (w/v) glycerol buffer. Data are represented as the mean residue ellipticities (MRE) and were calculated using the equation:

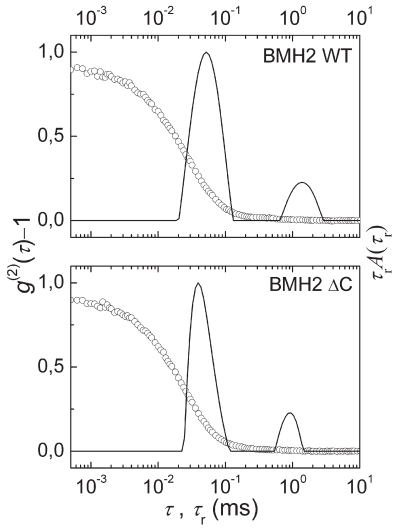


FIGURE 2: Dynamic light scattering. The autocorrelation functions, $g^{(2)}(\tau)$, of DLS from BMH2 WT and BMH2 ΔC solutions ($c$ = 4 mg/mL) (open circles) and the corresponding relaxation time distribution functions from the CONTIN analysis (solid line).

$$\mathrm{MRE} = \frac{\theta_{obs} \times 100 \times M_w}{clN_R} \quad (11)$$

where $\theta_{obs}$ is the observed ellipticity in degrees, $c$ is the protein concentration in milligrams per milliliter, $l$ is the path length in centimeters, $M_w$ is the protein molecular weight, and $N_R$ is the number of amino acids in the protein.

## RESULTS

*The C-Terminal Segment of BMH Proteins Exhibits Unfolded Conformation Compared to the Human 14-3-3ζ Isoform*. The principle aim of this study was to investigate the conformation of the C-terminal segments of yeast 14-3-3 protein isoforms BMH1 and BMH2. The BMH proteins possess a distinctly different C-terminus, which is longer and contains the polyQ sequence, compared to the 14-3-3 protein isoforms from higher eukaryotes (Figure 1B). The functional importance of these differences is currently unknown. It is now well established that the C-terminal segment of 14-3-3 proteins plays an important regulatory role by functioning as an autoinhibitor which occupies the ligand binding groove and blocks the binding of inappropriate ligands (*7*−*9*). Whether the same holds true or not for the yeast isoforms is unclear.

First, we used dynamic light scattering (DLS), time-resolved fluorescence anisotropy decay measurements, and size exclusion chromatography (SEC) to compare the molecular size of BMH proteins, the human 14-3-3ζ isoform, and their C-terminally truncated versions. To prepare the C-terminally truncated mutants (ΔC) of BMH1, BMH2, and 14-3-3ζ, a stop codon was inserted on positions Met237, Ile237, and Asp231, respectively. Throughout the measurement of the diffusion coefficient, the DLS gives access to the hydrodynamic radius of proteins, which depends on their size and their shape. A typical autocorrelation function, $g^{(2)}(\tau)$, obtained by DLS measurements is shown

Table 1: Hydrodynamic Radii of the Proteins from DLS and Sedimentation Velocity (SV) Experiments

| protein | BMH1 WT | BMH1 ΔC | BMH2 WT | BMH2 ΔC | 14-3-3ζ WT | 14-3-3ζ ΔC |
|---|---|---|---|---|---|---|
| $R_H$, Å (DLS)[a] | 44.9 ± 0.9 | 36.0 ± 0.4 | 43.3 ± 0.4 | 37.9 ± 0.3 | 37.3 ± 0.3 | 34.6 ± 0.2 |
| $R_H$, Å (SV)[b] | 40.0 ± 1.0 | 35.2 ± 0.8 | 40.9 ± 0.8 | 34.1 ± 0.7 | 37.6 ± 0.6 | 33.0 ± 1.0 |

[a]Values are the mean ± SD of five measurements in 20 mM Tris-HCl (pH 7.5), 150 mM NaCl, and 2 mM 2-mercaptoethanol. [b]Uncertainties are the standard errors from least-squares fits.

in Figure 2 together with the corresponding relaxation time distribution $A(\tau_r)$ from the CONTIN analysis. The obtained distribution functions consisted of an intensive fast mode and a weak slow mode (less than 20% of the overall scattering intensity), which can be ascribed to diffusive motion of protein molecules and diffusive motion of aggregates, respectively. (One has to keep in mind that the scattering power of the large aggregates is much higher that of the protein molecules, so that even a trace amount of the aggregates in the sample contributes significantly to the overall scattering intensity.) A shift of $A(\tau_r)$ to shorter relaxation times resulting in smaller $R_H$ is clearly visible after the BMH2 protein truncation.

The hydrodynamic radii ($R_H$), obtained from $\langle\tau_r\rangle$ of the fast mode of the CONTIN distributions using eq 3, were found to be independent of the protein concentration in the concentration range of 1.5−4 mg/mL (from 50 to 133 $\mu$M). The $R_H$ values measured by DLS are summarized in Table 1. For BMH1 WT and BMH2 WT the $R_H$ values obtained were 45 and 43 Å, respectively, whereas for BMH ΔC mutants were around 36−38 Å, which is also the value obtained for 14-3-3ζ WT. In the case of the 14-3-3ζ ΔC the $R_H$ of 35 Å was obtained. It is evident that the removal of the C-terminal segment significantly reduced the hydrodynamic radii of both BMH proteins but had small effect on the size of the 14-3-3ζ protein molecule.

The second method we used to compare the molecular size of BMH and 14-3-3ζ molecules was the measurement of time-resolved fluorescence anisotropy of AEDANS-labeled proteins. The relatively long excited-state lifetime of the AEDANS group (13−16 ns) enabled us to monitor the rotational diffusion of the BMH and 14-3-3ζ molecules with sufficient accuracy (*14*). Results of the SVD-MEM analysis are summarized in Table 2. Anisotropy decays were rather complex, exhibiting four classes of correlation times. Short correlation times located near 800 ps and 3 ns reflect fast local motion of the AEDANS group. The longest correlation time, $\phi_4$, belongs to extremely slow rotational diffusion of a fraction of large aggregates that were inevitably present in a small amount in our samples. With the AEDANS fluorescence lifetime around 15 ns it was not feasible to accurately determine the $\phi_4$ value. Importantly, the third correlation time, $\phi_3$, can be assigned to the rotational diffusion of a free BMH and 14-3-3ζ molecule. According to the well-known Stokes−Einstein−Debye (SED) relation the rotational correlation time of a rigid spherical rotor undergoing a Brownian rotational motion in a continuous isotropic solvent scales with its solvated volume $V$ according to the equation:

$$\Phi = \eta V/kT \quad (12)$$

where $\eta$ is solvent viscosity, $T$ the absolute temperature, and $k$ the Boltzmann constant (*17*, *21*). Thus $\phi$ gives information about the apparent solvated molecular volume and its hydrodynamic radius. Fluorescence anisotropy decays of asymmetric molecules modeled as prolate ellipsoids of revolution exhibit more correlation times related to rotational diffusion along different molecular axes. It is generally difficult to resolve them even in much simpler systems. However, as the molecular axial ratio increases, values of the new correlation components increase as well (*17*). Shifts of $\phi_3$ can therefore be well attributed to a combined change of molecular weight and molecular shape upon the C-terminal truncation. Consistently with the DLS data, the decrease of $\phi_3$ upon the removal of the C-terminal strongly suggests that native BMH proteins are distinctly larger or significantly more asymmetric than their C-terminally truncated mutants. Removal of the C-terminal segment did not have significant effect on the apparent hydrodynamic size of the 14-3-3ζ molecule.

Table 2: Summary of Time-Resolved Fluorescence Anisotropy Decay Measurements of BMH and 14-3-3ζ Proteins Labeled with AEDANS

| protein | $\beta_1$ | $\Phi_1$ (ns) | $\beta_2$ | $\Phi_2$ (ns) | $\beta_3$ | $\Phi_3$ (ns) | $\beta_4$ | $\Phi_4$ (ns) |
|---|---|---|---|---|---|---|---|---|
| BMH1 WT | 0.048 | 0.8 | 0.047 | 3.6 | **0.048** | **19** | 0.027 | ∞ |
| BMH1 ΔC | 0.047 | 0.7 | 0.045 | 2.6 | **0.060** | **14** | 0.019 | ∞ |
| BMH2 WT | 0.032 | 0.7 | 0.044 | 3.5 | **0.059** | **20** | 0.029 | ∞ |
| BMH2 ΔC | 0.046 | 0.8 | 0.035 | 2.9 | **0.060** | **12** | 0.034 | ∞ |
| 1433ζ WT | 0.035 | 0.8 | 0.037 | 3.0 | **0.063** | **15** | 0.035 | ∞ |
| 1433ζ ΔC | 0.031 | 0.8 | 0.043 | 3.0 | **0.064** | **15** | 0.026 | ∞ |

The size exclusion chromatography (SEC) elution profiles revealed similar results as DLS and fluorescence anisotropy measurements (Figure 3). The BMH1 WT and BMH2 WT elute significantly sooner compared to the C-terminally truncated mutants BMH1 ΔC and BMH1 ΔC whose elution volumes are comparable with those of 14-3-3ζ WT and 14-3-3ζ ΔC. Taken together, these results strongly suggest that the hydrodynamic apparent sizes of BMH proteins are significantly larger compared to the human 14-3-3ζ protein. The removal of the C-terminal segment causes BMH ΔC molecules to hydrodynamically behave similarly to the 14-3-3ζ protein. Similar hydrodynamic size of the 14-3-3ζ and 14-3-3ζ ΔC molecules is consistent with the fact that the C-terminal segment of the 14-3-3ζ protein molecule is in the absence of the ligand folded and located within the ligand binding groove (*9*). Therefore, it is reasonable to speculate that the C-terminal segment of the BMH protein either induces formation of bigger oligomers than dimers (e.g., tetramers) or adopts a widely opened and extended conformation that does not fold into the ligand binding groove, thus increasing asymmetry and the apparent molecular size of BMH proteins.

*Sedimentation Equilibrium and Sedimentation Velocity Experiments*. To investigate the former and for the 14-3-3 protein isoform unusual possibility of the higher oligomer formation, we determined the molecular masses of BMH proteins and their C-terminally truncated mutants using sedimentation equilibrium (SE) and sedimentation velocity (SV) experiments. Analysis of the SE and SV data revealed that BMH1 WT and BMH2 WT form stable dimers with molar masses of 61 kDa and 64 kDa, respectively (Table 3 and Figure 4). The sedimentation measurements were also performed with the C-terminally truncated BMH mutants 14-3-3ζ WT and 14-3-3ζ ΔC for comparison (Table 3). Since the values of molar mass of BMH proteins

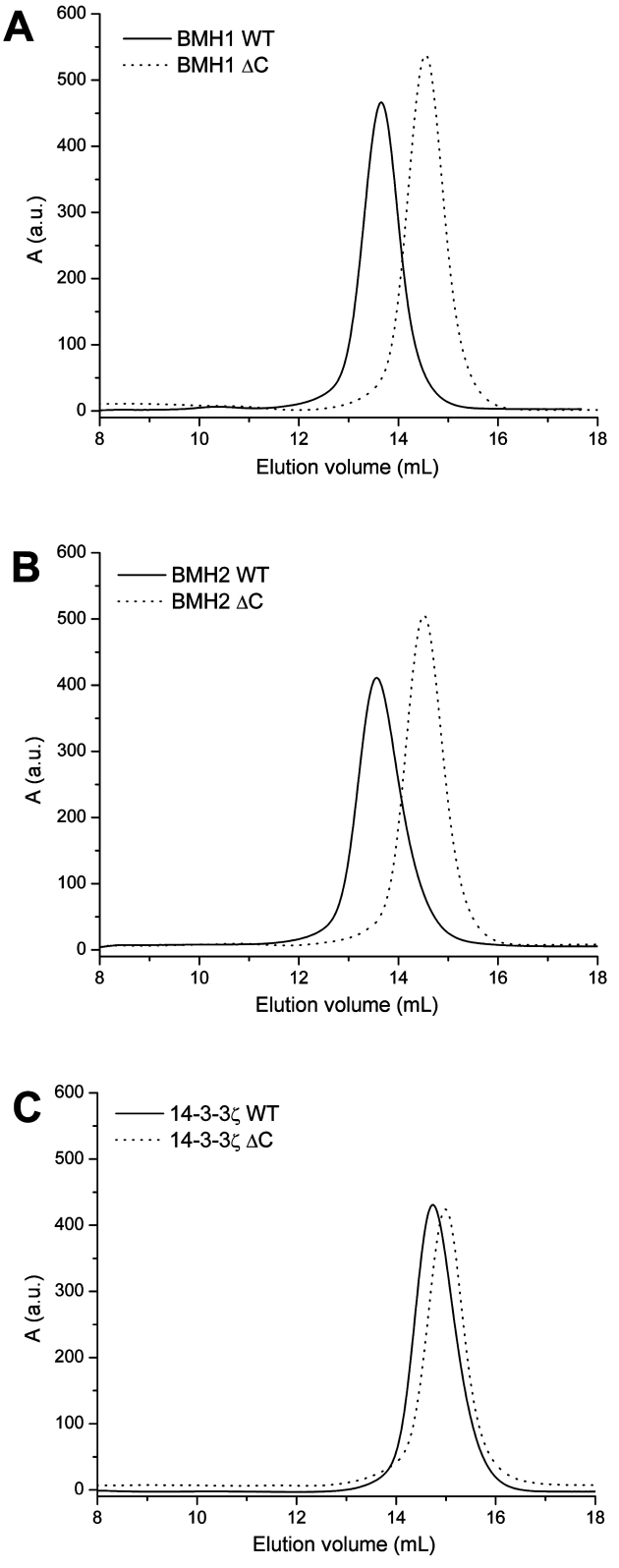


FIGURE 3: Size exclusion chromatography profiles. Size exclusion chromatography experiments were performed at a flow rate of 0.5 mL/min on a Superdex 200 HR 10/30 column (Amersham Biosciences) in buffer containing 20 mM Tris-HCl (pH 7.5), 200 mM NaCl, 1 mM EDTA, and 5 mM DTT. Samples contained BMH1 WT and BMH1 ΔC (A), BMH2 WT and BMH2 ΔC (B), 14-3-3ζ WT and 14-3-3 ΔC (C).

obtained from the sedimentation analysis correspond well with the theoretical masses calculated for dimers, it is possible to conclude that the C-terminal segment of BMH proteins does not induce formation of higher oligomers but rather adopts an open extended conformation that is responsible for the higher hydrodynamic radius of BMH molecules (Table 1). In addition, the hydrodynamic radii ($R_H$) of all studied proteins were calculated from the sedimentation velocity data. The $R_H$ values obtained from the sedimentation analysis are comparable to the DLS results and show that the removal of the C-terminal segment causes decrease in the hydrodynamic radii of all three studied proteins (Table 1).

*Ligand Binding Does Not Change the Conformation of the C-Terminal Segment of BMH Proteins*. Our previous experiments strongly suggest that the C-terminal segment of the BMH protein adopts extended conformation, thus likely being located outside of the ligand binding groove. This would implicate that the C-terminus of BMH proteins does not function as an autoinhibitor as has been described for mammalian or plant 14-3-3 protein isoforms. To further explore these differences, we investigated the effect of ligand (phosphopeptide pRaf-259) binding on the conformation of the C-terminal segment using time-resolved fluorescence intensity and anisotropy decay measurements of a single tryptophan residue inserted into the C-terminus of BMH2 at two different positions (Trp243 and Trp264). The tryptophan residues were placed either at the beginning or the end of the polyQ sequence (Figure 1B). Other tryptophan residues of BMH2 were mutated to phenylalanine. The pRaf-259 is a synthetic phosphopeptide containing a Raf-1 kinase sequence surrounding Ser259, which is a well-characterized 14-3-3 binding motif (*5*, *22*). The BMH WT proteins bind this peptide with $K_D$ of ~290 nM (Figure 5). The removal of the C-terminal segment does not have any significant effect on binding affinity of BMH proteins. In addition, the CD spectroscopy was used to check whether the truncation affects the secondary structure of 14-3-3 proteins. The comparison of obtained CD spectra revealed no significant changes upon the C-terminal segment removal (Figure 6).

Results of time-resolved tryptophan emission experiments are summarized in Table 4. Neither lifetime distribution patterns (data not shown) nor mean fluorescence lifetimes, $\tau_{mean}$, show any significant changes upon the binding of pRaf-259. Because Trp emission rates sensitively reflect variations in both polarity of its microenvironment and interactions, such result strongly indicates that binding of pRaf-259 did not induce conformational changes of the C-terminal that would affect the microenvironment of the fluorophore. Further, we investigated mobility of the fluorophore by the time-resolved fluorescence anisotropy. Raw anisotropy decays of BMH2 W243 and W264 mutants in the presence and absence of the ligand are shown in Figure 7. Visual inspection of the figure suggests that the ligand binding has a negligible effect on the anisotropy decay curves; i.e., local mobility of the Trp residue and the neighboring protein segment is independent of the pRaf-259 binding for both mutants. Taking into account noise in the data, the marginal difference in fitted curves of the BMH2 W264 mutant in the presence and absence of the ligand seems to be insignificant. From Figure 7 we can also conclude that Trp243 is significantly less mobile than downstream located Trp264. This can be judged from the lower depolarization of the BMH2 W243 emission and the higher anisotropy values at longer times after excitation. Fitted parameters of the anisotropy curves are presented in Table 4. Two short correlation times $\phi_1$ and $\phi_2$ and their amplitudes correspond to the fast local and segmental motion of the chromophore. Rather short fluorescence lifetime of the tryptophan residues, relatively high mobility of the C-terminal, and a small fraction of

Table 3: Molar Mass Values Calculated from Sedimentation Equilibrium (SE), Sedimentation Velocity (SV), and AEDANS Fluorescence Anisotropy Experiments

| $M_w$ ($\times 10^3$) | BMH1 WT | BMH1 ΔC | BMH2 WT | BMH2 ΔC | 14-3-3ζ WT | 14-3-3ζ ΔC |
|---|---|---|---|---|---|---|
| SE[a] | 61 ± 1.0 | 56 ± 2.0 | 64 ± 2.0 | 55 ± 1.0 | 55 ± 2.0 | 53 ± 2.0 |
| SV[a] | 61 ± 2.0 | 55 ± 1.0 | 63 ± 2.0 | 53 ± 1.0 | 59 ± 2.0 | 51 ± 2.0 |
| theoretical[b] | 60.7 | 54.0 | 62.7 | 54.2 | 56.1 | 53.1 |
| AEDANS[c] | 55−73 | 41−54 | 58−77 | 35−46 | 44−58 | 44−58 |

[a]Calculated weight-average molar mass using nonlinear least-squares analysis for a model assuming one ideal solute. Uncertainties are the standard errors from least-squares fits. [b]Molar mass calculated from amino acid sequence. [c]Orientational range of molecular masses calculated from $\phi_3$ (Table 2) and eq 12 using a mean specific protein volume of 0.73 mL/g and a hydration range from 0 to 0.23 mL of $H_2O$/g of protein (*17*, *23*).

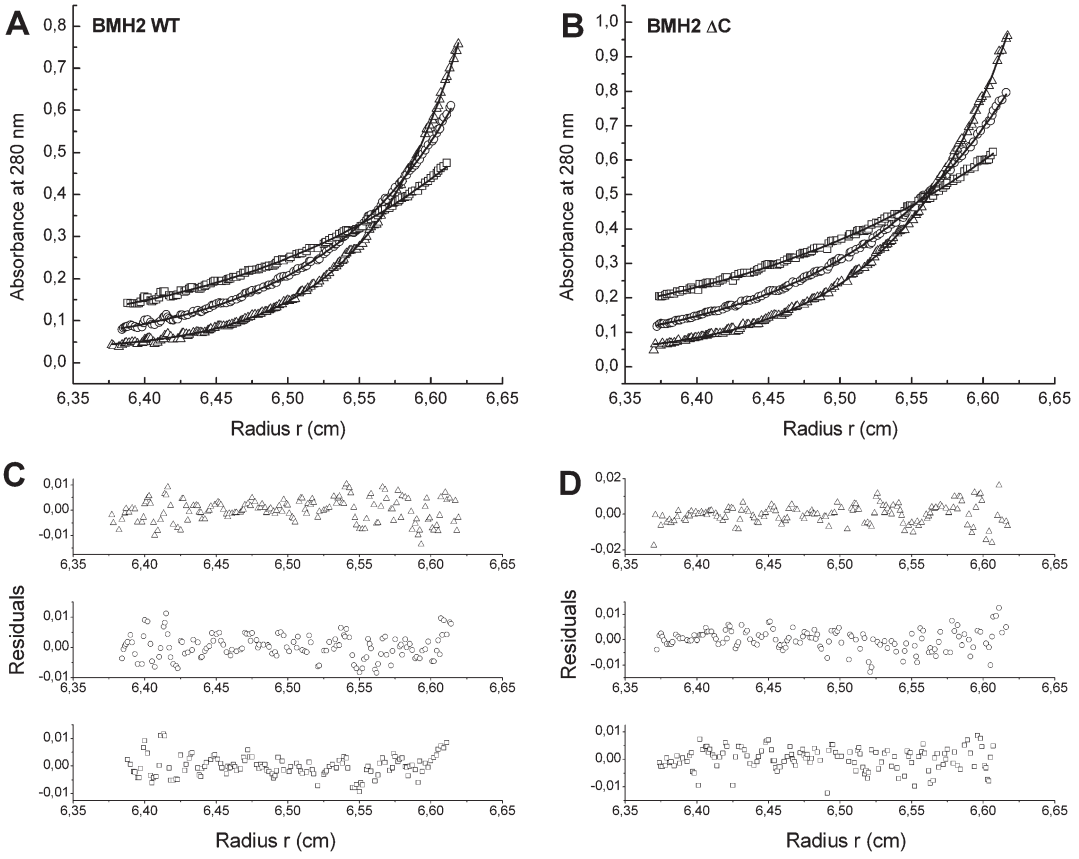


FIGURE 4: Sedimentation equilibrium measurements. (A, B) Sedimentation equilibrium profiles at 280 nm and 4 °C for BMH2 WT and BMH2 ΔC. Symbols correspond to data collected at 10500 (squares), 13500 (circles), and 16500 (triangles) rpm. The lines through the data represent the best fit in terms of one ideal solute. (C, D) Residuals corresponding to the best fit analysis in terms of one ideal solute. Data were analyzed using the SEDFIT and SEDPHAT packages (*15*, *16*).

higher aggregates inevitably present in the sample did not allow to accurately resolve the rotational correlation time corresponding to the rotational diffusion of the whole molecule. Nevertheless, the presented data strongly support our hypothesis that the C-terminal segment of BMH proteins does not block their ligand binding grooves and can therefore hardly function as an autoinhibitor. Immobilization of the C-terminal in the binding groove would certainly result in a significant change of the anisotropy decay shown in Figure 7 as was reported for the 14-3-3ξ protein (*8*).

## DISCUSSION

Numerous studies have revealed the importance of the C-terminal segment of 14-3-3 protein isoforms from higher eukaryotes in the regulation of the ligand binding (*7*−*10*). The C-terminal segment functions as an autoinhibitor which occupies the ligand binding groove and blocks the binding of inappropriate (e.g., unphosphorylated) ligands. The yeast 14-3-3 isoforms (BMH1 and BMH2) possess distinctively different C-terminal segments: they are longer and contain polyQ sequences of unknown function (Figure 1B). Therefore, it is possible that the C-terminal segments of yeast 14-3-3 isoforms might behave in a different way compared to the isoforms from higher eukaryotes. In this work, we used several biophysical techniques to investigate the conformational behavior of the C-terminal segments of BMH proteins.

Since the polyQ repeats are well-known to cause the protein aggregation (*12*), we first studied the molecular size of BMH proteins with and without their C-terminal segments. The hydrodynamic data gathered from these experiments indicate that molecules of BMH WT proteins are distinctly larger or significantly more asymmetric compared to human 14-3-3ζ WT, even though they do not differ too much in theoretical molar

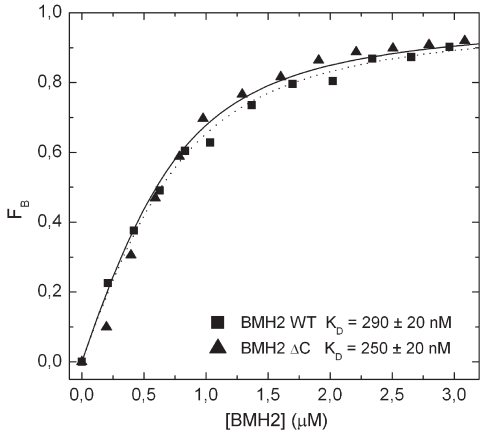


FIGURE 5: Fluorescence anisotropy-based binding assay. Fluorescence anisotropy binding assay was performed using a synthetic phosphopeptide pRaf-259 labeled at the N-terminus with fluorescein (*8*). Binding studies were performed with BMH2 WT (■) and BMH2 ΔC (▲). The $K_D$ was calculated using eq 5.

mass (Figures 2 and 3, Tables 1 and 3). The removal of the C-terminal segment significantly reduced the hydrodynamic radii obtained from the DLS and SV experiments of both BMH proteins and also increased their SEC elution volumes. On the other hand, it had small effect on the size of the 14-3-3ζ protein molecule, suggesting native BMH proteins either form higher oligomers or their molecules are significantly more asymmetric than their C-terminally truncated mutants. The results from AUC, however, clearly showed that the C-terminal segment does not cause higher oligomerization of BMH proteins (Table 3 and Figure 4). The molar masses obtained from the sedimentation equilibrium analysis confirmed the dimeric nature of all tested proteins. This indicates that the C-terminal segments of BMH proteins have markedly open and extended conformation which increases their hydrodynamic radius ($R_H$).

Time-resolved AEDANS fluorescence anisotropy decay measurements revealed that the third correlation time $\phi_3$ representing the rotation the whole protein (Table 2) and giving us the information about its apparent size is larger for BMH1 and BMH2 WTs than for their ΔC mutants. Reduction of the correlation time after the C-terminal truncation is larger than it would correspond to a reduction of the molecular mass. The ratio of molecular masses before and after the protein truncation $R = M_w/M_w(\Delta C)$ is equal to corresponding molecular volumes $V/V(\Delta C)$. For spherical proteins, according to eq 12, it also holds true that $R = V/V(\Delta C) = \phi_3/\phi_3(\Delta C)$. From $M_w$ in Table 3 we obtain that $R$ is around 1.1 for BMH proteins and even lower for 14-3-3ξ. Table 2 reveals that $\phi_3/\phi_3(\Delta C) \sim 1.4$, 1.7, and 1.0 for BMH1, BMH2, and 14-3-3ξ, respectively. This result suggests that the observed reduction of the apparent hydrodynamic size of BMH proteins is caused rather by decreased asymmetry of BMH molecules after the removal of the C-terminal segment than by decreased molecular mass. This conclusion fully agrees with our vision of an extended C-terminal segment of BMH proteins being located outside the ligand binding groove.

Our previous work on human 14-3-3ζ revealed that, in the absence of the ligand, the C-terminal segment of human 14-3-3ζ occupies the ligand binding groove of the 14-3-3 molecule with the negatively charged residues within the segment mimicking the negative charge of the phosphate group (*8*, *9*). The phosphopeptide binding changes the conformation of the C-terminal segment and displaces it from the ligand binding groove. However, our

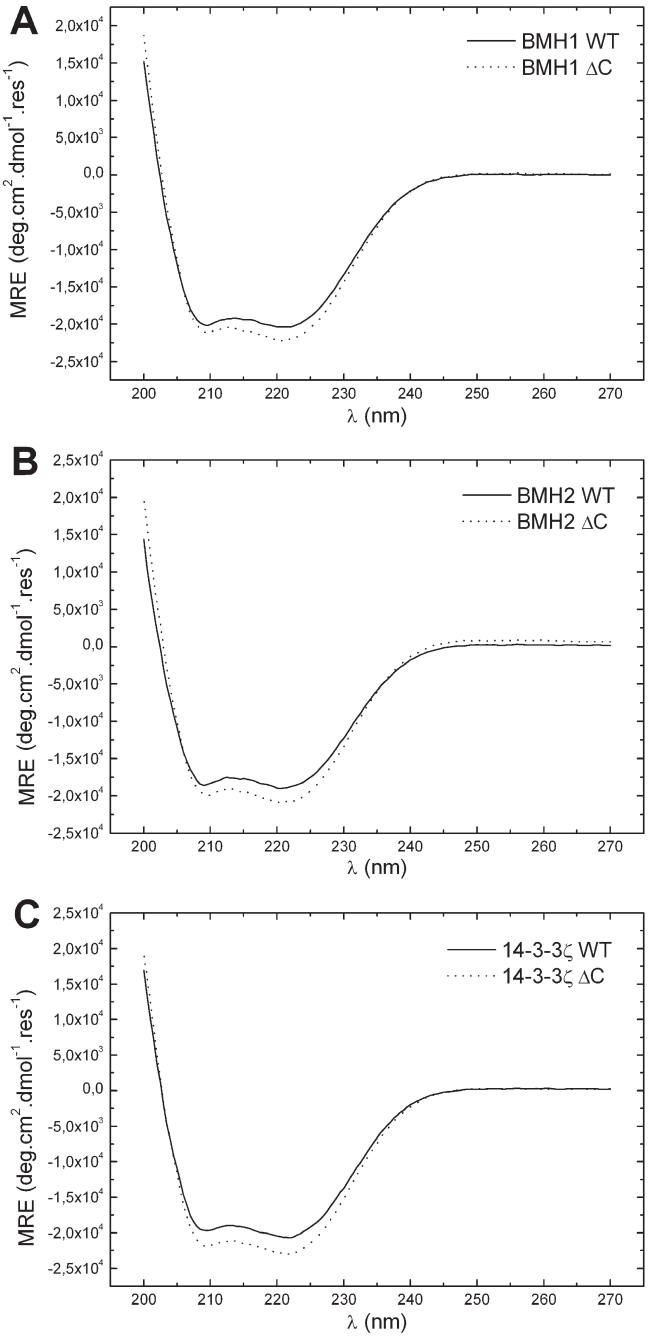


FIGURE 6: Circular dichroism spectroscopy of BMH and 14-3-3 proteins. The mean residue ellipticity (MRE) is plotted as a function of wavelength for BMH1 (A), BMH2 (B), and 14-3-3ζ protein (C). Spectra of wild-type (WT) and truncated (ΔC) proteins are shown as solid and dotted lines, respectively.

hydrodynamic data strongly suggest that the C-terminal segment of BMH proteins is located outside of the ligand binding groove. In order to further study the conformational behavior of the C-terminal segment, we used time-resolved tryptophan fluorescence. These measurements revealed that neither lifetime distribution patterns (data not shown) nor mean fluorescence lifetimes, $\tau_{mean}$, show any significant changes upon the binding of pRaf-259. In addition, time-resolved fluorescence anisotropy measurements showed no effect of the ligand binding on the mobility of the tryptophan residues and the neighboring protein segment (Table 4 and Figure 7).

Taken together, all of these experiments show that the C-terminus of BMH protein has markedly different conformation compared

Table 4: Summary of Time-Resolved Tryptophan Fluorescence Measurements of BMH2 Single-Tryptophan Mutants

| sample | $\tau_{mean}$ (ns)[a] | $\beta_1$ | $\Phi_1$ (ns) | $\beta_2$ | $\Phi_2$ (ns) | $\beta_3$ | $\Phi_3$ (ns) |
|---|---|---|---|---|---|---|---|
| BMH2w243[b] | 2.92 | 0.023 | 0.2 | 0.109 | 1.1 | 0.088 | ∞ |
| BMH2w243 + pRaf-259 | 2.89 | 0.022 | 0.3 | 0.113 | 1.1 | 0.087 | ∞ |
| BMH2w264 | 3.65 | 0.077 | 0.3 | 0.103 | 1.2 | 0.042 | ∞ |
| BMH2w264 + pRaf-259 | 3.52 | 0.069 | 0.2 | 0.114 | 1.2 | 0.039 | ∞ |

[a]Standard deviation is better than 0.10 ns. [b]BMH2w243 and BMH2w264 denote BMH2 mutants containing a single Trp residue at positions 243 and 264, respectively.

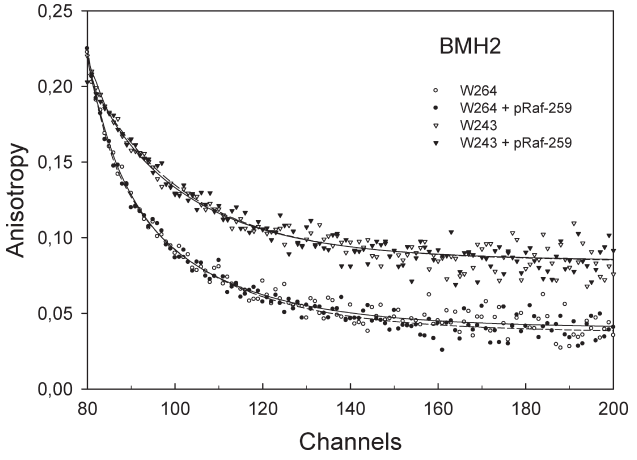


FIGURE 7: Tryptophan fluorescence anisotropy measurements. Fluorescence anisotropy decays of BMH2 W243 (triangles) and W264 (circles) in the presence (closed symbols) and absence (opened symbols) of pRaf-259 ligand. The time scale is 51 ps/channel.

to the human 14-3-3ζ isoform. Our results predict that this segment adopts an open and extended conformation without significant interaction with the ligand binding groove. Thus the C-terminal segment of BMH proteins can hardly function as an autoinhibitor.

## REFERENCES


1. Fu, H., Subramanian, R. R., and Masters, S. C. (2000) 14-3-3 proteins: structure, function, and regulation. *Annu. Rev. Pharmacol. Toxicol. 40*, 617–647.
2. Mackintosh, C. (2004) Dynamic interactions between 14-3-3 proteins and phosphoproteins regulate diverse cellular processes. *Biochem. J. 381*, 329–342.
3. Aitken, A. (2006) 14-3-3 proteins: a historic overview. *Semin. Cancer Biol. 16*, 162–172.
4. Xiao, B., Smerdon, S. J., Jones, D. H., Dodson, G. G., Soneji, Y., Aitken, A., and Gamblin, S. J. (1995) Structure of a 14-3-3 protein and implications for coordination of multiple signalling pathways. *Nature 376*, 188–191.
5. Muslin, A. J., Tanner, J. W., Allen, P. M., and Shaw, A. S. (1996) Interaction of 14-3-3 with signaling proteins is mediated by the recognition of phosphoserine. *Cell 84*, 889–897.
6. van Heusden, G. P. (2009) 14-3-3 proteins: insights from genome-wide studies in yeast. *Genomics 94*, 287–293.
7. Truong, A. B., Masters, S. C., Yang, H., and Fu, H. (2002) Role of the 14-3-3 C-terminal loop in ligand interaction. *Proteins 49*, 321–325.
8. Obsilova, V., Herman, P., Vecer, J., Sulc, M., Teisinger, J., and Obsil, T. (2004) 14-3-3zeta C-terminal stretch changes its conformation upon ligand binding and phosphorylation at Thr232. *J. Biol. Chem. 279*, 4531–4540.
9. Silhan, J., Obsilova, V., Vecer, J., Herman, P., Sulc, M., Teisinger, J., and Obsil, T. (2004) 14-3-3 protein C-terminal stretch occupies ligand binding groove and is displaced by phosphopeptide binding. *J. Biol. Chem. 279*, 49113–49119.
10. Shen, W., Clark, A. C., and Huber, S. C. (2003) The C-terminal tail of *Arabidopsis* 14-3-3omega functions as an autoinhibitor and may contain a tenth alpha-helix. *Plant J. 34*, 473–484.
11. van Heusden, G. P., and Yde Steensma, H. (2006) Yeast 14-3-3 proteins. *Yeast 23*, 159–171.
12. Ross, C. A., Poirier, M. A., Wanker, E. E., and Amzel, M. (2003) Polyglutamine fibrillogenesis: the pathway unfolds. *Proc. Natl. Acad. Sci. U.S.A. 100*, 1–3.
13. Obsil, T., Ghirlando, R., Klein, D. C., Ganguly, S., and Dyda, F. (2001) Crystal structure of the 14-3-3zeta:serotonin N-acetyltransferase complex. A role for scaffolding in enzyme regulation. *Cell 105*, 257–267.
14. Obsilova, V., Vecer, J., Herman, P., Pabianova, A., Sulc, M., Teisinger, J., Boura, E., and Obsil, T. (2005) 14-3-3 protein interacts with nuclear localization sequence of forkhead transcription factor FoxO4. *Biochemistry 44*, 11608–11617.
15. Houtman, J. C., Brown, P. H., Bowden, B., Yamaguchi, H., Appella, E., Samelson, L. E., and Schuck, P. (2007) Studying multisite binary and ternary protein interactions by global analysis of isothermal titration calorimetry data in SEDPHAT: application to adaptor protein complexes in cell signaling. *Protein Sci. 16*, 30–42.
16. Schuck, P. (2000) Size-distribution analysis of macromolecules by sedimentation velocity ultracentrifugation and Lamm equation modeling. *Biophys. J. 78*, 1606–1619.
17. Lakowicz, J. R. (1999) Principles of Fluorescence Spectroscopy, 2nd ed., Kluwer Academic/Plenum Publishers, New York.
18. Lacourciere, K. A., Stivers, J. T., and Marino, J. P. (2000) Mechanism of neomycin and Rev peptide binding to the Rev responsive element of HIV-1 as determined by fluorescence and NMR spectroscopy. *Biochemistry 39*, 5630–5641.
19. Bryan, R. K. (1990) Maximum-entropy analysis of oversampled data problems. *Eur. Biophys. J. 18*, 165–174.
20. Vecer, J., and Herman, P. (2010) Maximum entropy analysis of analytically simulated complex fluorescence decays, J. Fluoresc. (DOI 10.1007/s10895-009-0589-1).
21. Lavalette, D., Tetreau, C., Tourbez, M., and Blouquit, Y. (1999) Microscopic viscosity and rotational diffusion of proteins in a macromolecular environment. *Biophys. J. 76*, 2744–2751.
22. Yaffe, M. B., Rittinger, K., Volinia, S., Caron, P. R., Aitken, A., Leffers, H., Gamblin, S. J., Smerdon, S. J., and Cantley, L. C. (1997) The structural basis for 14-3-3:phosphopeptide binding specificity. *Cell 91*, 961–971.
23. Murphy, L. R., Matubayasi, N., Payne, V. A., and Levy, R. M. (1998) Protein hydration and unfolding—insights from experimental partial specific volumes and unfolded protein models. *Folding Des. 3*, 105–118.
24. Rittinger, K., Budman, J., Xu, J., Volinia, S., Cantley, L. C., Smerdon, S. J., Gamblin, S. J., and Yaffe, M. B. (1999) Structural analysis of 14-3-3 phosphopeptide complexes identifies a dual role for the nuclear export signal of 14-3-3 in ligand binding. *Mol. Cell 4*, 153–166.
25. Chenna, R., Sugawara, H., Koike, T., Lopez, R., Gibson, T. J., Higgins, D. G., and Thompson, J. D. (2003) Multiple sequence alignment with the Clustal series of programs. *Nucleic Acids Res. 31*, 3497–3500.